GRAZING INCIDENCE X-RAY DIFFRACTION

Dutta, P.

Dept. of Physics & Astronomy, Northwestern University, Evanston, IL 60208-3112 USA

Abstract

X-rays have been used for decades to study the structure of bulk crystalline materials: they interact with matter weakly conpared to (say) electrons, and thus they are not normally thought of as surface-sensitive. However, in recent years techniques have been devised that, in combination with the availability of intense collimated beams from synchrotron sources, have transformed X-rays into a versatile and powerful tool for the study of surfaces, monolayers and ultrathin films. This articles briefly describes the principles of grazing-incidence X-ray diffraction, and gives a few examples of results obtained using this technique.

Perhaps the most basic question in the materials sciences is, where are the atoms (or molecules)? The question is just as relevant for surface and monolayer studies as it is for studies of bulk materials, where X-rays have long been an essential characterization tool. X-rays interact weakly with matter, and this gives it a number of advantages: multiple scattering can often be neglected (unlike, say, electrons), and X-rays penetrate significant distances (typically of the order of 0.1-10 mm, depending on the material and the X-ray energy), allowing them to obtain microscopic structural information averaged over a large ensemble of atoms or molecules. This distinguishes X-ray techniques from imaging techniques such as the various scanning microscopies, which give real-space images but are limited to surfaces and interfaces, and where you can't have very high resolution and view a large, statistically significant area at the same time.

Now in this special issue we are concerned with surfaces and interfaces, and thus the advantages of X-rays for bulk studies would appear to be disadvantages. X-rays are not intrinsically a surface-selective probe. However, very intense sources of X-rays are now available, and it is sometimes possible to obtain surface information simply by looking for deviations from the ideal bulk scattering, and attributing these deviations to the surface. In other words, one scatters X-rays 'by brute force' from the entire sample, and looks for the small part of the scattering that is due to the surface. This is done primarily when the bulk is a good single crystal, because then the scattering from it is largely limited to Bragg peaks. The excess scattering between Bragg peaks can then be attributed to a reconstructed surface or an adsorbed monolayer. This is the basic idea of 'truncation rod' analysis, so called because the scattering due to a surface is in the form of rods normal to the surface, rather than Bragg points, in reciprocal space (see below).

This method has been used extensively in the study of surfaces of inorganic single crystals, and of monolayers and thin films deposited on these crystals [for reviews, see Refs. 1-3]. Its disadvantages are that the substrate must be a good single crystal with little scattering between Bragg peaks, and the truncation rod profiles must generally be fitted using assumed models in order to extract information, as in the case of reflectivity.

When the substrate is thin enough to be largely transparent to X-rays, as in the case of thinly-cleaved mica [4], or when there is a sample without a substrate, as in the case of freestanding liquid-crystal films [5], it is possible to look at the lateral structure by going right through the sample, as shown in Fig. 1. In the geometry shown, $\vec{K} = \vec{q} - \vec{q}'$ is in the plane of the surface or thin film; changing the incident and scattered angles allows the diffraction vector to move off the plane, for example to follow 'rods'. This geometry is rarely used, because very few substrates are sufficiently transparent to X-rays. A related case is that of high-surface-area polycrystalline substrates such as exfoliated graphite [6]; here, as in Fig.1, the surface-to-volume ratio is high, and the X-rays are sent right through the sample. However, the use of multiple, non-parallel surfaces creates a heterogeneous system and averaging over multiple orientations means that some information is lost.

The grazing incidence geometry (Fig. 2) , on the other hand, is surface selective, i.e. largely avoids scattering from the substrate, and it does not require a transparent substrate. This technique is based on the fact that at X-ray energies, the refractive index for most materials is slightly *less than* 1.0. One can therefore have total *external* reflection from a surface if the incident angle is small enough (typically 1-25 milliradians, or 0.05°-1.5°, depending on the substrate electron density and the X-ray

energy). At this point the substrate is not entirely invisible to X-rays, but only an

evanescent wave penetrates into and scatters from it. The X-ray intensity is therefore

highest at the surface, as desired. It is possible to increase the surface selectivity further

by reducing the incident angle and thus causing the evanescent wave to damp out faster.

Fig. 2 also shows a specular beam, but if the incident beam is coming in at less

than the critical angle for total reflection, the specular beam does not carry a whole lot of

useful information. However, if there is any lateral order at the surface (or in a

monolayer at the surface) there will be diffraction peaks. The diffracted beam need not

be observed only at grazing exit angles, but may be detected at any angle, resulting in a

$\vec{K}$ that has both horizontal and vertical components. As shown to the right side of Fig. 2,

if there is a two-dimensional lattice of points, the reciprocal lattice is a two-dimensional

lattice of rods (since there is no periodicity in the z-direction, all K_z are equivalent as far

as the Bragg condition is concerned). By ignoring K_z and locating the diffraction peaks

in K_x and K_y, the reciprocal lattice and thus the real lattice can be determined. Notice that

in the grazing-incidence geometry it is never possible to go to $K_z=0$, because this would

require that the incident and diffracted photons make zero angles to the surface.

However, a two-dimensional system is forgiving: the reciprocal lattice is in the form of

rods, and so the diffraction peaks can just as easily be located at slightly non-zero K_z.

(The scattering intensity will vary strongly along the rods if the lattice is not composed

of points but of molecules, and this intensity variation contains information regarding the

orientation of the molecules. This is discussed later in this paper.)

Of course, this technique has some limitations. The first is that it works well only

with very smooth surfaces, and not all surfaces can be made sufficiently smooth. If the

critical angle is 0.1°, for example, any long-range or short-range variation in the surface normal of the order of 0.1 ° will move large parts of the surface out of the total reflection condition. Second, at grazing angles, most of the incoming X-ray beam is wasted. Assuming an incident angle of 0.1 ° and a surface dimension of 1cm, only a 2Tm slice of the X-ray beam will fall on the surface; the rest either hits the side or passes over the sample. Unfortunately focussing, when possible, helps but also hurts; if the incident beam is converging to a focus at the sample, it contains a range of incident directions and therefore not all the photons will land below the critical angle for total reflection. The need is therefore for a beam that is intrinsically both compact and collimated. This is provided by synchrotron sources. Even with synchrotron radiation, further focussing is useful, but since this is done with large source-to-mirror and mirror-to-focus distances (not practical in the laboratory), the beam can be focussed without significantly worsening the divergence. (For the commonly used 1:1 focussing, the intrinsic small divergence of the synchrotron beam is turned into an equally small convergence.)

Even with the use of focussed synchrotron radiation, photons are lost in the grazing incidence geometry; very few synchrotron beam lines focus the radiation to a few Tm beam height. For this reason, many experiments described as being in the grazing incidence geometry actually use incident angles somewhat larger than the critical angle; this increases the number of incident photons. This is possible if their substrates are crystalline; as long as one stays away from the substrate Bragg peaks, there is very little substrate scattering. These are in effect experiments like those mentioned at the beginning of this article, where the surface scattering is seen in addition to the bulk scattering. The geometry shown qualitatively in Fig. 2 is still employed because it is a

way of getting $\vec{K}$ to be close to the surface plane, but no particular effort is made to achieve surface selectivity by having the incident beam fall on the sample at less than the critical angle. Unfortunately this does not work when the substrate is disordered and thus scatters in all directions (e.g. glass, silicon with native oxide, liquids).

In the rest of this article I will give some samples of our own work on Langmuir monolayers. This system requires 'true' grazing-incidence (below the critical angle) scattering because the substrate is water. At 8KeV, the critical angle is about 2.5 milliradians; even after vibration isolation we find that the surface normal varies by about ±0.5 milliradians due to capillary waves, and thus our incident angle must be kept under 2 milliradians.

Langmuir monolayers are spread on water using molecules with 'split personalities': one end is hydrophilic, while the rest is hydrophobic. This causes them to be isolated to the surface of water, with the hydrophilic end down and hydrophobic end up. Our studies have been largely focussed on saturated fatty acids, "physicists' molecules" that can be approximated as rods. The phase diagram of saturated fatty acid Langmuir monolayers was once thought to be simple, but, as a result of X-ray and other studies, is now frequently and appropriately described as 'rich'. A phase diagram showing eight of the observed phases (from Ref. 7) is shown in Fig. 3. The phases are commonly described in terms of:

(a) the horizontal-plane lattice, which may be hexagonal or distorted hexagonal (centered rectangular)---the distortion is exaggerated in the schematic diagrams in Fig 3;

(b) whether the molecules tilt, and if they tilt, the direction---this is indicated in the schematic diagrams by 'shadows' (where the molecules are vertical, only a round filled circular shadow is shown; where the molecules tilt, the shadow is extended with an open circle in the direction of the tilt);.

(c) the degree of positional order---the lowest-temperature phases in Fig. 3 appear to be long-range ordered, while the others are intermediate-range-ordered mesophases.

How do we know all this? It seems obvious that the lattice would emerge from the diffraction data, and the degree of order from the lateral peak widths, but what about the tilt angle and direction? We discussed earlier a 2D lattice of points. When the unit cells contain not points but molecules, the reciprocal lattice remains unaltered; it is composed of rods normal to the plane. However, now the intensity is not spread out uniformly along the rods; rather, it is determined by the form factor of the molecule, which in turn is determined by the structure of the molecule and its orientation. Consider the specific case of a cigar-shaped molecule, as shown in Fig. 2; this is a reasonable (but not perfect—see below) approximation for a saturated fatty acid. The form factor for such a molecule has the form of a disk, as shown to the lower right of Fig. 2. The disk and the molecule have a common axis, so when the molecule tilts, so does the disk. The maximum intensity along a rod occurs when the reciprocal disk intersects the rod. In general, this will happen at different places for different Bragg rods. This is shown in Fig. 4 for several different cases of interest. Of course, when the molecules are vertical, the diffraction maxima are in the plane. Remember that the lattice is (usually) not hexagonal but distorted-hexagonal (centered rectangular); thus there are two diffraction peaks, one of which is doubly degenerate, as shown to the left of Fig. 4. Langmuir

monolayers are powders in the plane, so that there is no way to distinguish K_x from K_y; there is only K_{xy}. The lowest panels show intensity contours in the K_z-K_{xy} plane; when the molecules are vertical, the maxima are in the plane, i.e. at K_z=0.

The two symmetry directions of this rectangular lattice are 90° away from each other; tilts in these directions are commonly known as NN (nearest-neighbor direction) and NNN (next-nearest neighbor direction) tilt. As the schematic diagrams in Fig. 4 show, for NN tilt the maxima is above the plane for two of three the first-order diffraction rods, and in the plane for the third. Actually the figure shows six rods, but three of the 2D lattice vectors are just the negatives of the other three. Maxima below the plane cannot be seen because the X-rays will not penetrate the water. Since the system is two-dimensional, there are only two basis vectors; any two of the three first-order Bragg vectors add (or subtract) to give the third. This imposes no particular condition on the three K_{xy}, but it means that the K_z values of the two peaks with lower K_z will add up to equal to K_z value of the peak at highest K_z. In the case of the NN tilt shown, one peak has K_z =0 and the other two have equal nonzero K_z, so this relationship is satisfied. In the case of NNN tilt (see diagram), all peaks have nonzero K_z, but th one with lower K_z is doubly degenerate and has exactly half the K_z of the higher peak. Again, this satisfies the requirement that the sum of the two smaller K_z values equal the largest. When the tilt is not in a symmetry direction, there will in general be three observable first-order peaks, none of them degenerate and all of them at nonzero K_z. This is shown to the right of Fig. 4.

We see all these phenomena in our diffraction data, and from the positions of the maxima in K_{xy} and K_z, we can precisely determine the tilt angle and direction. As an

example, Fig. 5 shows diffraction data from a Langmuir monolayer along an isotherm, from the L_2 to the L_2' phase (see Fig. 3 to identify phases).. At low pressures, the tilt is NN (cf. schematic in Fig. 4). At higher pressure, the tilt is NNN (cf. schematic in Fig. 4). At intermediate pressures, within a narrow range, we see three peaks, indicating an intermediate tilt direction. These are swivelling transitions; the molecules are chaging their tilt direction relative to the lattice, through an intermediate chiral phase not indicated in fig. 3. (Although non-chiral molecules may not form chiral structures in 3D, they are allowed to do so in 2D.) Further details, including a Landau-type theory, are in Ref. 8.

Earlier I listed the lattice, the tilt angle, and the tilt direction; it turns out that this list is not complete. The alkane chains are not actually 'cigars' with circular cross-sections; to fully specify how the molecules are arranged, one needs also the orientation of the molecule about its long axis. Since the carbon atoms in the alkane tail define a plane, specifying the orientation of this backbone plane is a convenient way to specify the orientation of the entire molecule.

Kaganer and coworkers [9-11] have developed an extensive Landau theory of Langmuir monolayers, which has been very successful in explaining many of the features of the observed phase diagram. Backbone ordering is a crucial component of their theoretical framework. Experimental methods for looking at backbone order are therefore very desirable. In single crystals where a large number of diffraction peaks can be observed, it is possible to deduce, from the peak intensities, the molecular orientation relative to the lattice. However, in Langmuir monolayers, even the second-order diffraction peaks are sometimes hard to locate. Recently [12], however, we were able to see a 'forbidden' peak resulting from a doubling of the unit cell. Fig. 6 shows diffraction

peaks for the high-pressure low-temperature CS phase indexed in terms of a rectangular non-primitive unit cell. We see not only the previously reported [13] first-order (11) and (20) peaks, and the previously reported [14] second-order (02) and (31) peaks, but a (21) peak. Now the rectangular unit cell contains two molecules, and if these molecules are identical, the (21) peak is forbidden. This immediately tells us that there are two inequivalent sites. This doubles the unit cell and will cause the (21) peak to be visible, but they will in general also cause the (01) peak to be visible; however we do not see the (01) peak. The absence of the (01) peak argues strongly for a herringbone arrangement of molecular cross-sections, just like some phases of paraffins. As can be seen from the inset to Fig. 6, the backbones at the two inequivalent sites make equal (although opposite) angles relative to the (01) direction; therefore the molecules at the two sites have identical structure factors for the (01) peak and this peak remains forbidden. However, relative to the (21) direction, the backbones at the two sites are oriented very differently (again, see inset); thus the two molecular structure factors are not the same and the (21) peak is not forbidden. (For the same reasons we expect that the (12) peak will be visible but the (10) peak will be forbidden for a herringbone structure. We did not look for either of these peaks.)

Similar results are obtained for the tilted L_2'' phase; these data are not shown here but can be found in ref. 12. However, in the other phases, we have been unable to see the (21) peak. This means that there is no long-range backbone order in these phases. Of course there may still be short-range backbone order. If the backbone plane orientations were completely disordered, the average cross-section would be circular, and one would get a hexagonal structure. This is what happens in the high-pressure high-temperature LS

or 'Rotator' phase. If the molecules are vertical, any distortion from the hexagonal structure in the horizontal plane implies that the backbones are lining up. Fig. 7 shows diffraction data (from ref. 15) along a high-pressure isobar, from the S phase to the LS phase. Distortion manifests itself as a splitting of the triply-degenerate first-order peak; if the distortion is along a symmetry direction, e.g. a near-neighbor (NN) or a next-nearest neigbor (NNN) direction, then there is one doubly degenerate and one non-degenerate peak, as is seen in the S phase. It is easily deduced from the peak positions that the hexagon is 'stretched' in an NN direction (or equivalently, compressed in the NNN direction) in the S phase. As the temperature increases, the peaks merge, via a very weakly distorted LS_I region to the hexagonal LS_{II} region. In other words, the high-pressure sequence of phases CS-S-LS causes the backbone order to go from long range to short range to zero.

The above discussion does not exhaust the topic of Langmuir monolayers, and of course it does not exhaust the topic of grazing-incidence diffraction. For more details of both topics, see the reviews by Kaganer, Möhwald and Dutta [7], and by Als-Nielsen et al [16]. In the last few years, grazing incidence diffraction has been used to study surface freezing in paraffin monolayers [17], self-assembled (chemisorbed) films on silicon [18] and gold [19,20], and self-assembled films on the surface of mercury [21]. There is also a review of thin inorganic film studies using this technique by Barbier et al [22].

REFERENCES

1.   Robinson, I.K. and Tweet, D.J., *Repts. Prog. Phys.* 1992, **55**, 599

2.   Robinson, I., Eng, P. and Schuster, E., *Acta Physica Polonica A*, 1994, *86*, 513

3.   Robinson, I.K., *Acta Cryst.* 1998, **54**, 772

4.   Prakash, M., Dutta, P., Ketterson, J.B. and Abraham, B.M. *Chem. Phys. Lett.,*
        1984, **111**, 395

5.   e.g. Demikhov, E.I,, Dolganov, V.K. and Meletov, K.P., *Phys. Rev. E.*, 1995, **52**,
        1285

6.   Thomy, A. and Duval, X., *Surf. Sci.*, 1994, **300**, 415

7.   Kaganer, V.M, Möhwald, H. and Dutta, P., *Revs. Mod. Phys.*,1999, **71**, 779

8.   Durbin, M.K., Malik, A., Richter, A.G., Ghaskadvi, R., Gog, T. and Dutta, P., *J.
        Chem. Phys.*, 1997, **106**, 8216

9.   Kaganer, V.M. and Indenbom, V.L., *J. Phys. II* , 1993, **3**, 813

10.   Kaganer, V.M. and Loginov, E.B., *Phys. Rev. Lett.* 1993, **71**, 2599; Kaganer, .M.
        and Loginov, E.B., *Phys. Rev. E*, 1995, **51**, 2237

11.   Kaganer, V.M. and Osipov, M.A., *J. Chem. Phys.,* 1998, **109**, 2600

12.   Durbin, M.K., Richter, A., Yu, C.J., Kmetko, J., Bai, J.M. and Dutta, P., *Phys.
        Rev. E*, 1998, **58**, 7686

13.   Lin, B., Shih, M.C., Bohanon, T.M., Ice, G.E, and Dutta, P., *Phys. Rev. Lett.*,
        1990, **65**, 191

14.   Bohanon, T.M., Lin, B., Shih, M.C., Ice, G.E. and Dutta, P., *Phys. Rev. B,* 1990,
        41, 4846

15. Shih, M.C., Bohanon, T.M., Mikrut, J.M., Zschack, P. and Dutta, P., *Phys. Rev. A,* 1992, **45**, 5734

16. Als-Nielsen, J., Jacquemain, D., Kjaer, K., Leveiller, F., Lahav, M. and Leiserowitz, L., *Phyics Reports* 1994, **246**, 252

17. Ocko, B.M., Wu, X.Z., Sirota, E.B., Sinha, S.K., Gang, O. and Deutsch, M., *Phys. Rev. E*, 1997, **55**, 3164

18. Tidswell, I.M., Rabedeau, T.A., Pershan, P.S., Kosowsky, S.D., Folkers, J.P. and Whitesides, G.M., *J. Chem. Phys.* 1991, **95**, 2854

19. Fenter, P., Eberhardt, A., Liang, K.S. and Eisenberger, P., *J. Chem. Phys*., 1997, **106**, 1600

20. Fenter, P., Schreiber, F., Zhou, L., Eisenberger, P. and Forrest, S.R., *Phys. Rev. B*., 1997, **56**, 3046

21. Magnussen, O.M., Ocko, B.M., Deutsch, M., Regan, M.J., Pershan, P.S., Abernathy, D., Grubel, G. and Legrand, J.F., *Nature*, 1996, **250**, 384

22. Barbier, A., Renaud, D., Robach, O., and Guenard, P., *J. de Physique IV*, 1998, **8**, 203

FIGURE CAPTIONS

Fig. 1   A transmission geometry for looking at the lateral structure of a surface or thin film.

Fig. 2   (a) schematic diagram of a grazing-incidence X-ray diffraction experiment; (b) 'Rods' formed in reciprocal space by a two-dimensional lattice of points, and the "reciprocal disk" of an extended molecule, which combine to give the diffraction pattern from a 2D array of extended molecules. [From ref. 7]

Fig. 3   Generic phase diagram for fatty acid Langmuir monolayers, schematically showing the qaulitative lattice distortions and tilt directions determined by X-ray diffraction data. [From ref. 7.]

Fig. 4   Real- and reciprocal-space views, amd characteristic diffraction patterns, from (left to right) an untilted phase, a nearest-neighbor-tilted (NN) phase, a next-nearest-neighbor-tilted (NNN) phase; and (f) intermediate-tilted phase. [From ref. 7]

Fig. 5   diffraction data from a fatty acid monolayer at various pressures. [From ref. 8.]

Fig. 6   Sample x-ray data (in the horizontal plane, i.e. at $K_z\approx0$) from a heneicosanoic ($C_{21)}$ acid monolayer in the CS phase (T=7°C, π=30 dyn/cm). Peaks are indexed according to a centered orthorhombic lattice with two molecules per unit cell. The inset shows a centered orthorhombic lattice with a herringbone arrangement of the molecular backbones. [From ref. 12.]

Fig. 7   Diffraction data in the horizontal plane, from heneicosanoic ($C_{21)}$ acid monolayers along a 31 dyn/cm isobar. The solid lines are fits using one or two Lorentzians, as appropriate; the dotted lines are individual Lorentzians. [From ref. 15.]
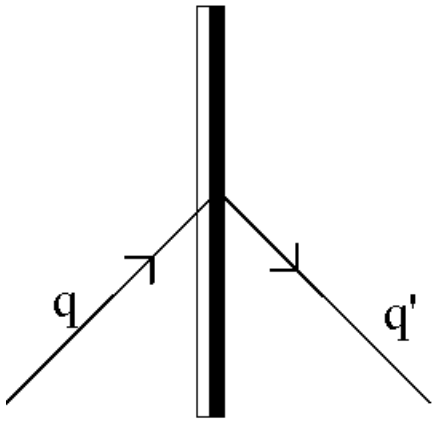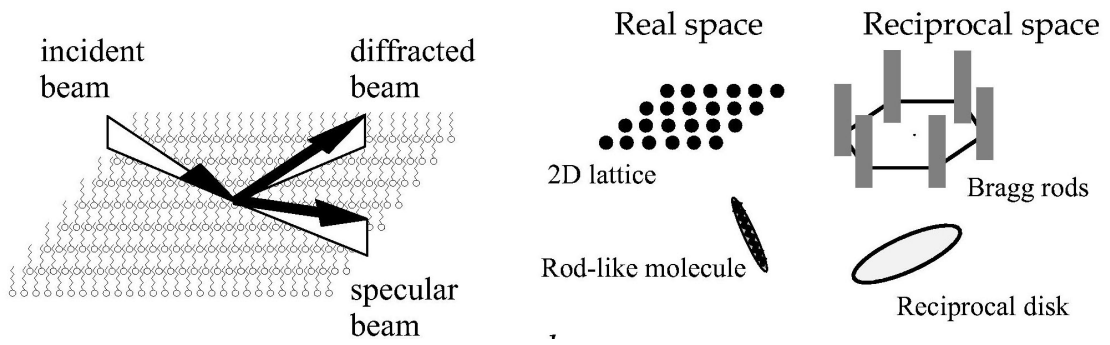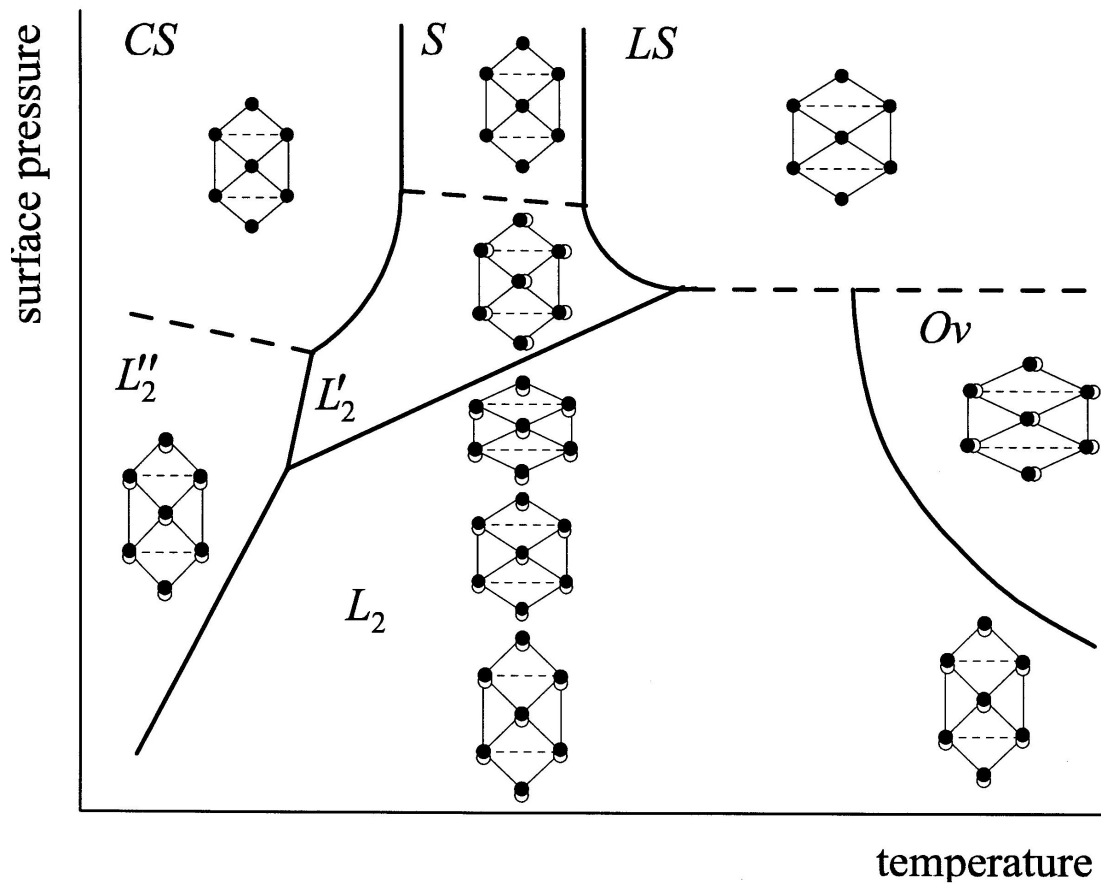
q   q'

Fig. 1

incident
beam

diffracted
beam

specular
beam

Real space

Reciprocal space

2D lattice

Rod-like molecule

Bragg rods

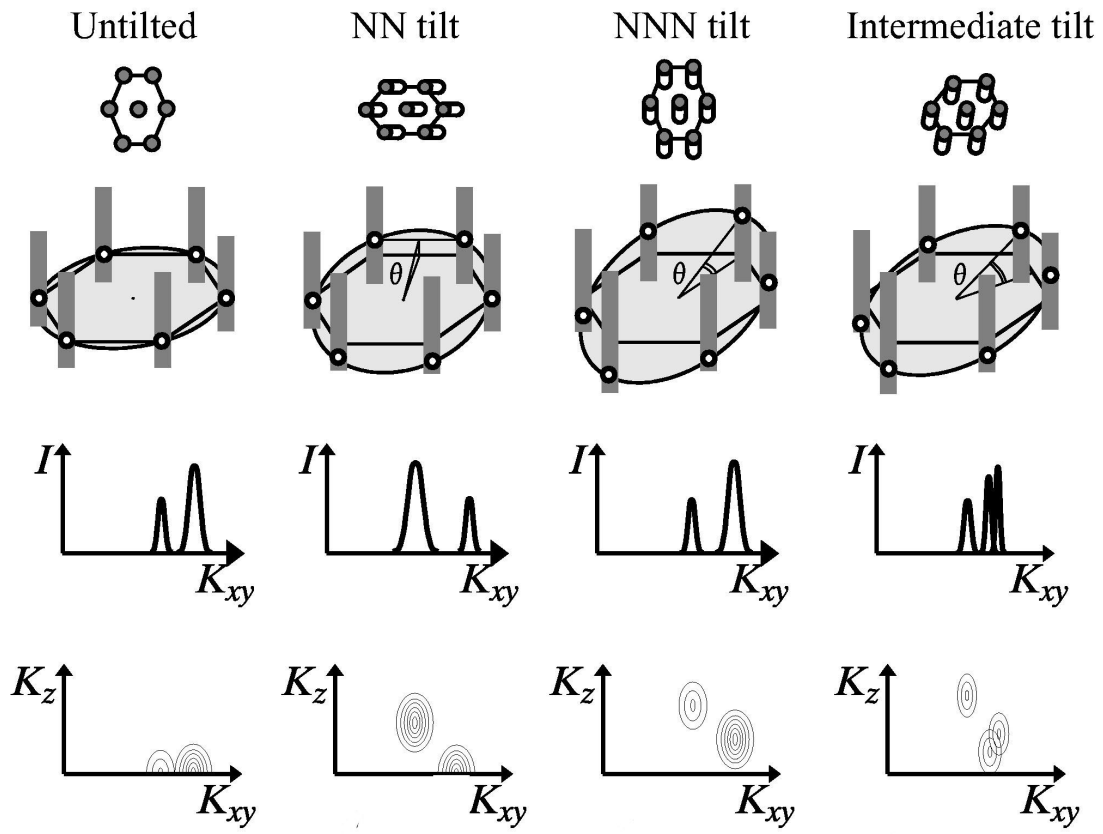Reciprocal disk

Fig. 2

Fig. 3

Untilted NN tilt NNN tilt Intermediate tilt

Fig. 4

Fig. 5

Fig. 6

Fig. 7